Accepted version of the article published in 2018 19th IEEE International Workshop on Signal Processing Advances in Wireless Communications (SPAWC).
DOI: 10.1109/SPAWC.2018.8446026. Available at: http://ieeexplore.ieee.org

Uncoordinated Space-Frequency Pilot Design for Multi-Antenna Wideband Opportunistic Communications

Jordi Borràs and Gregori Vazquez
Department of Signal Theory and Communications, Technical University of Catalonia (UPC)
Building D5, Campus Nord UPC, Jordi Girona 1-3, 08034 Barcelona, Spain
Email: {jordi.borras.pino, gregori.vazquez}@upc.edu

***Abstract*—The statistical side information of interference channels is exploited in this paper to derive a novel uncoordinated on-line pilot design strategy for opportunistic communications. Assuming a time division duplex (TDD), or frequency division duplex (FDD) with feedback, wireless network and reciprocity, we prove that the space-frequency pilot design technique in terms of minimum cross-interference to external-network users reduces to a classical minimum-norm problem. The advantages of this novel methodology are time-domain invariance to noise-subspace rotations, a maximally flat angle-frequency response, and robustness in front of frequency calibration errors. Simulation results are reported to assess the performance of the proposed strategy and the advantages of its low-resolution quantization in low signal-to-noise ratio (low-SNR) regimes.**

***Index Terms*—Opportunistic communications, pilot and waveform design, multi-antenna systems, distributed networks, wideband regime.**

I. Introduction

The wireless spectrum scarcity is a well-identified bottleneck for future wireless networks. The expected growth of the number of interconnected wireless interfaces and the demanded high data-rates can make unfeasible the communication whether the resources are not properly exploited.

In this sense, opportunistic communications [1] have recently centered attention in wireless communications. Techniques such as dynamic spectrum access [2] or cognitive radio [3] have been widely studied as a possible solution to overcome the expected over-congestion of wireless networks. It is worth pointing out that additional information can be found in references therein.

Furthermore, the use of multiple antennae is able to provide precoding flexibility, in order that a better knowledge of the protected-users network (denoted as external network in this work) spatial occupation is achieved. Hence, the opportunistic-users network (here, internal network) opportunistically transmit exploiting the unused spatial degrees-of-freedom (DOF) induced by using antenna arrays.

Regardless the use or not of antenna arrays, orthogonal frequency-division multiplexing (OFDM) is so far the most common modulation in opportunistic communications (see [4] and references therein). However, other alternatives are explored in the literature. For instance, noise subspace-based waveforms are used to precode opportunistic signals. The main dissemblance between different strategies is that side information may be acquired statistically [5], [6], imperfectly [7–9] or instantaneously [10–12]. References therein are suggested to the reader for further information.

It is worth noting that an important issue is how the opportunistic channel is estimated and how other modulation parameters are set. In this sense, there are two classical approaches: centralized or distributed methods (see [13] and references therein). Notice that the latter does not suffer from the inefficiencies of backbone communication.

Pilot sequences are used to sense the channel and establish a consensus on which resources are being used between internal transmitting and receiving nodes in order to minimize as much as possible the cross-interference delivered to external networks (see [14] and references therein). Commonly, pilots are known sequences at each system end and hence are designed in an ad-hoc manner using off-line methods. However, centralized pilot design procedures present some inaccuracies such as sensitivity to frequency errors and they are not adapted to each scenario.

Concerning the latter, in this work we present an on-line pilot design method for multi-antenna opportunistic communications operating in the wideband regime. This procedure is based on the statistical side information of interference channels. Each internal node designs its own pilot reference signals by solely using local external-network observations. It is finally important to notice that the presented methodology also applies for distributed adaptive scenario-aware waveform design in opportunistic communications.

This paper is organized as follows: in Sec. II we describe the signal model used throughout this paper. In Sec. III we analyze the design technique, denoted as *beam-dimension spreading*, which is optimal in terms of minimum cross-interference. Moreover, some properties of this technique are briefly discussed. In Sec. IV we numerically assess the performance of the derived pilots, and its low-resolution quantization as well.

II. Signal Model

Let us consider an heterogeneous external network composed of M users. Each user radiates wideband signals with

This work has been supported by the Spanish Ministry of Economy, Industry and Competitiveness through project WINTER: TEC2016-76409-C2-1-R (AEI/FEDER, UE), and the Catalan Government (AGAUR) under grant 2017 SGR 578.

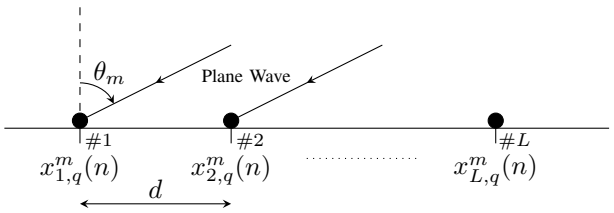

Fig. 1. Uniform Linear Array (ULA) used by internal users. Note that θ_m denotes the direction-of-arrival (DOA) with respect to the broadside.

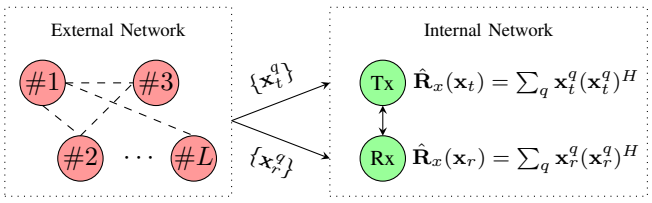

Fig. 2. Point-to-point opportunistic communication based on uncoordinated pilot design using external-network local observations.

a spectral support $B_m = [f_L^{(m)}, f_H^{(m)}]$ for $m = 1, \ldots, M$, smaller than the system bandwidth B, and impinges an internal user with a direction belonging to the set $\Theta = \{\theta_m\}_{1 \leq m \leq M}$. The preceding space-frequency sensing stage is out of the scope of this work.

Each internal user is equipped with a uniform linear array (ULA) composed by $L > M$ elements and tapped delay-lines of N filters. Truly, there are several models for the wideband signals impinging internal-users' array.

For the sake of convenience, in this paper we model $x^{(m)}_{\ell,q}(n)$ according to Fig. 1, i.e., the q-th snapshot observed from the m-th external user at the ℓ-th element as the sum of Z_m monochromatic plane waves

$$x^{(m)}_{\ell,q}(n) = \sum_{z=1}^{Z_m} a^{(z)}_m \exp\left\{ j2\pi f^{(m)}_z ((\ell-1)\tau_m + n) \right\} + w^{(m)}_{\ell,q}(n) \tag{1}$$

with $\ell = 1, \ldots, L$ and $n = 0, \ldots, N-1$. In (1), $a^{(z)}_m$ stands for the Fourier coefficient of the m-th external user at the z-th frequency and $\tau_m = \frac{d}{c}\sin(\theta_m)$, where d is the inter-element spacing and c is the propagation speed. Moreover, $w^{(m)}_{\ell,q}(n)$ is the temporally and spatially uncorrelated noise term. Without loss of generality, we assume $w^{(m)}_{\ell,q}(n) \sim \mathcal{CN}(0, \sigma^2_w)$. Then, the contribution of all external users is just the addition in (1) for $m = 1, \ldots, M$.

In order to write the snapshots in a convenient manner, we define the temporal and spatial steering vectors as

$$\begin{aligned} \boldsymbol{\nu}^{(m)}_z &= [1 \;\; \exp\{2\pi f^{(m)}_z\} \cdots \exp\{2\pi f^{(m)}_z (N-1)\}]^T, \\ \boldsymbol{\omega}^{(m)}_z &= [1 \;\; \exp\{2\pi f^{(m)}_z \tau_m\} \cdots \exp\{2\pi f^{(m)}_z \tau_m (L-1)\}]^T, \end{aligned}$$

where $(\cdot)^T$ stands for transpose operator. Then, the q-th snapshot can be written as

$$\mathbf{x}_q = \sum_{m,z} a^{(z)}_m \underbrace{\left(\boldsymbol{\nu}^{(m)}_z \otimes \boldsymbol{\omega}^{(m)}_z \right)}_{\mathbf{s}_{m,z}} + \mathbf{w}_q, \tag{2}$$

with $\mathbf{s}_{m,z}$ referring to the spatio-temporal steering vector and $\otimes$ stands for the Kronecker tensor product. By appropriately arranging these steerings in the so-called steering matrix $\mathbf{S} \in \mathbb{C}^{NL \times D}$, where the number of occupied DOFs is defined as

$$D = \sum_{m=1}^{M} Z_m, \tag{3}$$

the q-th snapshot in (2) can be written in matrix form as follows

$$\mathbf{x}_q = \mathbf{S}\mathbf{a} + \mathbf{w}_q, \tag{4}$$

where $\mathbf{a} \in \mathbb{C}^D$ is the Fourier coefficients vector. In the following, we will consider $q = 1, \ldots, Q$ observed snapshots.

III. Joint Beam and Dimension Spreading-based Uncoordinated Pilot Design

A. Problem Formulation

In this work, we address the uncoordinated design of spatio-temporal pilots. As depicted in Fig. 2, each internal node will only use its local external-network observations to design its pilot. Notice that, for the sake of simplicity, we consider a point-to-point opportunistic transmission.

In order not to interfere the external-network communication, internal nodes can only exploit the available DOFs $K = NL - D$. Hence, the internal transmitted pilot will be given by

$$\mathbf{y}(t) = \sum_n a[n] \boldsymbol{\varphi}(t - nT_p), \tag{5}$$

where $a[n]$ denotes a known pseudorandom sequence of size P of a given constellation. It is noteworthy that this sequence should spread the pilot signal power spectral density in order to avoid spectral lines. Despite the transmitted pilot is composed of a pseudorandom sequence and a pulse shaping filter $\boldsymbol{\varphi}(t) \in \mathbb{C}^{NL}$, this work deals solely with the optimization of $\boldsymbol{\varphi}(t)$. Finally, T_p is the pilot period. Recalling the definition of spatio-temporal snapshots (2), it is worth noting that $\boldsymbol{\varphi}(t)$ exploits both spatial and temporal domains.

Further on we assume each internal user has sensed the Spatio-Temporal Power Spectral Density (ST-PSD) from the external network, $\phi_x(\vartheta; f)$. Thus, our objective is

$$\boldsymbol{\varphi}_{\text{opt}}(t) = \arg\min_{\boldsymbol{\Phi}} \int_B \int_{-\frac{\pi}{2}}^{\frac{\pi}{2}} \phi_x(\vartheta; f) |\Phi(\vartheta; f)|^2 \mathrm{d}\vartheta \mathrm{d}f, \tag{6}$$

where $\boldsymbol{\varphi}_{\text{opt}}(t)$ is the designed spatio-temporal pilot at an arbitrary internal node and $\boldsymbol{\Phi} = \mathcal{F}^2[\boldsymbol{\varphi}(t)]$, denoting $\mathcal{F}^2[\cdot]$ the 2D Fourier Transform. Thus, we tackle the pilot design minimizing the spatio-temporal overlapping between the internal-network transmission and the external network.

Unfortunately, due to noisy measurements, shadowing and/or multipath fading, internal users will sense the external-network ST-PSD with an uncertainty, i.e.,

$$\tilde{\phi}_x(\vartheta; f) = \phi_x(\vartheta; f) - \xi(\vartheta; f), \tag{7}$$

in such a way that some occupied directions and frequencies are shadowed at that internal node. The peak of estimation errors in (7) is upper-bounded by a certain constant $|\xi(\vartheta; f)| \leq \epsilon$. This uncertainty $\xi(\vartheta; f)$ will cause a residual cross-interference

between internal and external transmissions. In order to account for the worst-case cross-interference, (6) becomes

$$\min_{\mathbf{\Phi}} \left\{ \int_B \int_{-\frac{\pi}{2}}^{\frac{\pi}{2}} \tilde{\phi}_x(\vartheta; f) |\Phi(\vartheta; f)|^2 \mathrm{d}\vartheta \mathrm{d}f + \epsilon \int_B \int_{-\frac{\pi}{2}}^{\frac{\pi}{2}} |\Phi(\vartheta; f)|^2 \mathrm{d}\vartheta \mathrm{d}f \right\}. \quad (8)$$

It is worth noting that the optimization problem in (8) has to be tackled under minimum-norm criterion, which is equivalent to total least-squares method [15]. In the time domain, the cost function in (8) can be written in terms of the sensed external-network autocorrelation matrix $\hat{\mathbf{R}}_x$ as

$$\min_{\boldsymbol{\varphi}} \max_{\mathbf{\Delta}} \left\{ \boldsymbol{\varphi}^H (\hat{\mathbf{R}}_x + \mathbf{\Delta}) \boldsymbol{\varphi} \right\}, \quad (9)$$

where $\mathbf{\Delta}$ is a positive semi-definite matrix that accounts for the DOFs uncertainty and $(\cdot)^H$ stands for the conjugate transpose operator. In this case, the upper-bound on DOFs uncertainty is $\|\mathbf{\Delta}\|_F \leq \epsilon$, being $\|\cdot\|_F$ the Frobenius norm.

As discussed in [6], when the worst case is taken into consideration, the error matrix $\mathbf{\Delta}$ indicates that all occupied DOFs are shadowed, providing then the maximum cross-interference to external users. Thus, minimizing the norm of the designed pilot is the best that can be done to achieve the highest performance under the worst conditions.

Thus, in order to achieve the minimum spatio-temporal spectral overlapping, the designed pilot must be orthogonal to the external-network signal subspace, which is exhibited in the sensed autocorrelation matrix as $\hat{\mathbf{R}}_x = \hat{\mathbf{R}}_s + \hat{\mathbf{R}}_n$. Hence, the pilot optimization problem addressed in this work can be expressed as

$$\boldsymbol{\varphi}_{\text{opt}} = \arg\min_{\boldsymbol{\varphi}} \|\boldsymbol{\varphi}\|^2 \text{ s.t. } \hat{\mathbf{R}}_s^H \boldsymbol{\varphi} = \mathbf{0} \text{ and } \boldsymbol{\varphi}^H \mathbf{e}_k = 1, \quad (10)$$

with $\mathbf{e}_k \triangleq [\underbrace{0 \ldots 0}_{NL-k} \ 1 \ \underbrace{0 \ldots 0}_{k-1}]^T$. It is noteworthy that in (10) we have imposed a non-trivial design constraint that will be further optimized.

B. Beam-Dimension Spreading Technique

With the observations described in (4), each internal user may estimate the noisy spatio-temporal spectrum as

$$\hat{\mathbf{R}}_x = \frac{1}{Q} \sum_{q=1}^{Q} \mathbf{x}_q \mathbf{x}_q^H, \quad (11)$$

If there are available DOFs, i.e., $K \neq 0$, the external-network signal presents a low-rank autocorrelation matrix which admits the following eigendecomposition

$$\hat{\mathbf{R}}_x = \hat{\mathbf{U}}_s \left(\hat{\mathbf{\Lambda}}_s + \sigma_w^2 \mathbf{I}_D \right) \hat{\mathbf{U}}_s^H + \sigma_w^2 \hat{\mathbf{U}}_n \mathbf{I}_K \hat{\mathbf{U}}_n^H, \quad (12)$$

where $\hat{\mathbf{U}}_s$ and $\hat{\mathbf{U}}_n$ contain the eigenvectors that span the signal and noise subspaces, respectively. $\hat{\mathbf{\Lambda}}_s$ is a diagonal matrix containing the D signal eigenvalues, and σ_w^2 is the noise variance. Here, $\mathbf{I}_D$ and $\mathbf{I}_K$ stand for the identity matrices of size D and K, respectively.

It is worth pointing out that, in wideband regime, the eigenanalysis of $\hat{\mathbf{R}}_x$ is not as straightforward as in narrowband regime. However, some authors have studied how to decompose the autocorrelation matrix into signal and noise subspaces (see, e.g., [16–18]). In this work, we have considered the approach stated in [18], i.e., denoting r_s the rank of the noiseless external-network aggregate autocorrelation matrix, if $r_s < NL$ then $\hat{\mathbf{R}}_x - \sigma_w^2 \mathbf{I}_{NL}$ will be low-rank, and then we can easily discern when a given pair $(\hat{\lambda}_i, \hat{\mathbf{u}}_i)$ belongs to signal ($\mathcal{S}$) or noise ($\mathcal{N}$) subspaces, which are defined as

$$\mathcal{S} = \left\{ (\hat{\lambda}_i, \hat{\mathbf{u}}_i) \ : \ 1 \leq i \leq r_s \right\}, \quad (13a)$$

$$\mathcal{N} = \left\{ (\hat{\lambda}_i, \hat{\mathbf{u}}_i) \ : \ r_s < i \leq NL \right\}. \quad (13b)$$

Given the orthogonality exhibited between the signal and noise subspaces, we may write our spatio-temporal pilot as a linear combination of noise eigenvectors, i.e., $\boldsymbol{\varphi} = \hat{\mathbf{U}}_n \boldsymbol{\lambda}$. Hence, the Lagrangian associated to (10) is

$$\mathcal{L}(\boldsymbol{\lambda}, \mu) = \boldsymbol{\lambda}^H \hat{\mathbf{U}}_n^H \hat{\mathbf{U}}_n \boldsymbol{\lambda} + \mu(1 - \boldsymbol{\lambda}^H \hat{\mathbf{U}}_n^H \mathbf{e}_k). \quad (14)$$

Thus, the pursued pilot has the following structure

$$\tilde{\boldsymbol{\varphi}}_k = \frac{1}{\alpha_k} \hat{\mathbf{P}} \mathbf{e}_k, \quad (15)$$

where $\hat{\mathbf{P}} \triangleq \hat{\mathbf{U}}_n \hat{\mathbf{U}}_n^H$ is the noise subspace projector and $\alpha_k \triangleq \mathbf{e}_k^H \hat{\mathbf{P}} \mathbf{e}_k$ refers to the k-th entry of noise-subspace projector's main diagonal. The derivation of (15) is omitted due to length limitations (cf. [6]). It can be proven that the optimality of (15) is achieved for

$$k_{\text{opt}} = \max_k \ [\hat{\mathbf{P}}]_{k,k}. \quad (16)$$

The optimal pilot is nothing but the minimum norm solution presented in the seminal paper [19]. Therefore, the optimal pilot presents some interesting properties which are being briefly discussed below.

1) Time-domain invariance to rotations: The pilot proposed in (15) relies on the noise subspace projector. Let $\mathbf{\Omega}$ be a rotation matrix, such that $\mathbf{\Omega}\mathbf{\Omega}^H = \mathbf{I}_K$ and $\det(\mathbf{\Omega}) = \pm 1$. Then, the rotated noise subspace projector $\hat{\mathbf{P}}_r = \hat{\mathbf{U}}_n \mathbf{\Omega}\mathbf{\Omega}^H \hat{\mathbf{U}}_n^H$ remains equal to $\hat{\mathbf{P}}$ if a rotation within the noise subspace occurs. Thus, the derived pilot (15) exhibits invariance to rotations yielding coherent detection.

This property is of a paramount importance in the time domain since the solution in (15) avoids ambiguity between the adopted transmission and reception vectorial basis. Despite it also holds in the spatial domain, ambiguity between two different DOAs has not practical sense.

2) Spectral whiteness: The non-trivial constraint used in (10) implies the linear predictor condition presented in [20]. Thus, the polynomial roots of the optimal pilot present an almost uniform distribution exhibited by the extraneous zeros as in [21]. The proof of this property is omitted due to space limitations. Further details on the proof of the frequency-domain spectral whiteness can be found in [6].

The interest of this property in the spatial domain arises when the internal users do not know their exact location, and then isotropically radiating information increases the probability of achieving the destination.

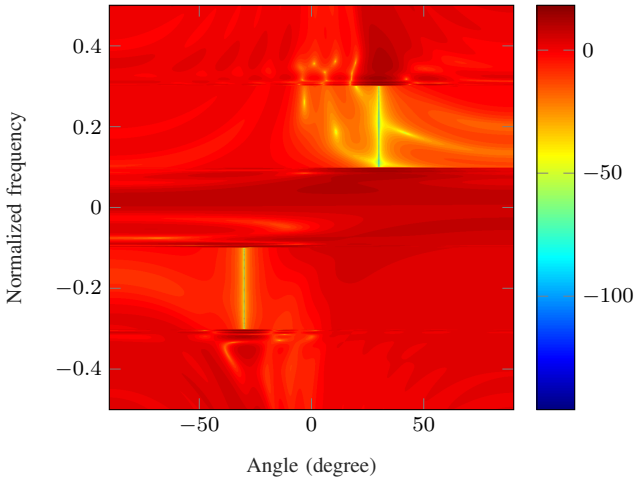

Fig. 3. Spatio-Temporal Power Spectral Density of the frequency-dependent optimal beamvector derived in (15) at internal transmitting node.

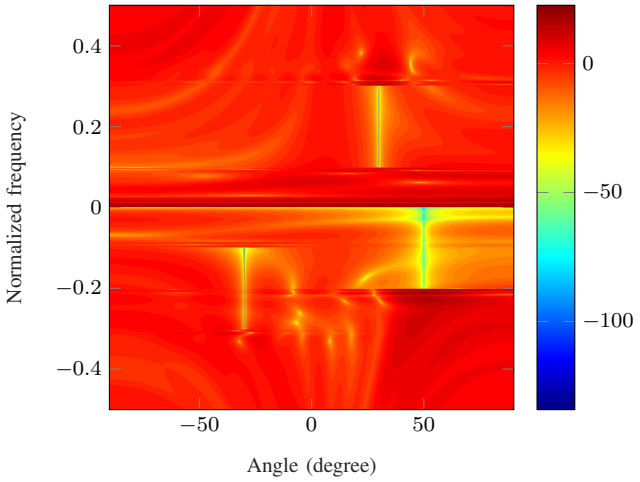

Fig. 4. Spatio-Temporal Power Spectral Density of the frequency-dependent optimal beamvector derived in (15) at internal receiving node.

3) Robustness in front of frequency errors: In classical *off-line* pilot generation schemes, each system end is sensitive to frequency errors. Contrariwise, in the proposed *on-line* scenario-adapted technique, since the designed pilots are solely based on local external-network observations, each end is locally self-calibrated, avoiding hence a centralized frequency reference unprotected to calibration errors.

IV. Simulation Results

In this section we present a toy example to illustrate the performance of the proposed solution. Both internal transmitter and receiver are equipped with a ULA of 16 half-wavelength spaced elements. The tapped-delay line associated to each array element is composed by 1024 filters.

A. Scenario Description

For this example, we consider a 3-user heterogeneous external network. Each user radiates wideband signals of the same bandwidth, but with different spectral support.

Due to shadowing and/or multipath fading, the internal transmitter senses only two external users, whereas the receiver senses the three ones. The scenario is summarized in Table 1.

TABLE I
Scenario parameters for the toy example.

	User 1		User 2		User 3	
	B_1	θ_1	B_2	θ_2	B_3	θ_3
TX	$[-0.3,-0.1]$	-30º	$[0.3,0.1]$	30º	Shadowed	
RX	$[-0.3,-0.1]$	-30º	$[0.3,0.1]$	30º	$[-0.2,0]$	50º

B. Performance Assessment

In Fig. 3 and Fig. 4 we present the pilot designed at internal transmitter and receiver, respectively. Notice that our proposal tries to uniformly distribute the power among all available spatio-temporal spectral resources, i.e., the available DOFs are used in an almost uniform manner. We observe how each internal node leaves unused the sensed occupied DOFs.

The power spectral density of the designed pilot at each internal node evaluated at different DOAs is depicted in Fig. 5. As well, the power angular density radiated by each internal user evaluated at the central frequency of each spectral support is reported in Fig. 6. Notwithstanding the scaling factor, subtle shaping differences, and the lack of coordination between both internal nodes, we appreciate that the internal-pilot attenuations at the occupied DOFs perfectly match.

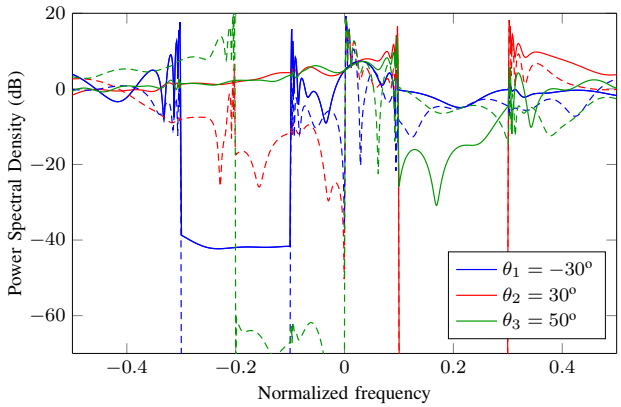

Fig. 5. Power Spectral Density (PSD) for different DOA. Here, solid lines indicates the PSD at transmitter, whereas dashed lines refers to PSD at receiver.

C. Low-SNR Regime Performance

We define the signal-to-noise ratio (SNR) per DOF as

$$\mathsf{SNR}_k \triangleq \frac{S_T}{N_0}\frac{1}{K} = \frac{\mathsf{SNR}}{K}, \quad \text{for } k = 1,\ldots,K, \tag{17}$$

being S_T the finite power budget, N_0 the noise power, and SNR the system SNR. Hence, for a large number of available DOFs K, our operating regime tends to the low-SNR regime. It could be a great advantage in terms of computational complexity, since we can quantize the received transformed-domain signals with a few number of bits. Let $\mathcal{Q}_b(\cdot)$ be the b-bit quantization function and $\mathbf{z}$ be a complex-valued signal. The quantized version of $\mathbf{z}$ is then $\tilde{\mathbf{z}} = \mathcal{Q}_b(\mathbb{Re}[\mathbf{z}]) + j\mathcal{Q}_b(\mathbb{Im}[\mathbf{z}])$, being $\mathbb{Re}[\cdot]$ and $\mathbb{Im}[\cdot]$ the real and imaginary parts, respectively. For

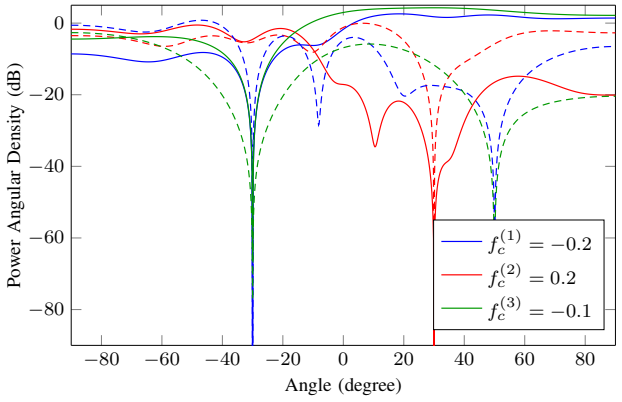

Fig. 6. Power Angular Density (PAD) at the m-th user central frequency $f_c^{(m)}$. Solid and dashed lines refer to transmitter and receiver, respectively.

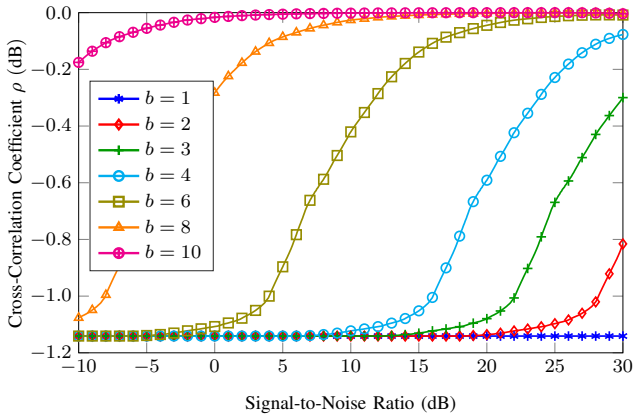

Fig. 7. Cross-correlation coefficient ρ between unquantized and quantized pilots as a function of the system SNR for different quantization bits, considering $L = 16$ elements and tapped delay-lines of $N = 1024$ filters.

this experiment, we have considered a uniform quantization with $b = \{1, 2, 3, 4, 6, 8, 10\}$ bits (cf. [22]), with a normalized signal dynamics of $\pm 3\sigma$, where σ^2 is the power of the noisy signal. No changes are observed for $\pm 2\sigma$ nor $\pm\sigma$. In Fig. 7, we have analyzed the similarities between unquantized optimal pilot [see (15)] and the quantized pilots for different values of the system SNR [see (17)] by measuring the cross-correlation coefficient ρ between them. Notice that for very low SNR, the cross-correlation coefficient is roughly the same for all proposed quantizers, except when 10 quantization bits are used. In this case, the achieved performance is better than the offered by low-resolution quantizers.

V. Conclusions

This paper has addressed the uncoordinated pilot design for opportunistic communication exploiting second-order statistics of the external network. Minimum-norm has naturally arisen as the optimal design criterion in terms of minimum cross-interference. The pilot spreads transmitted signal over all available directions and frequencies, i.e. jointly performs beam and dimension spreading. The proposed pilot presents an angle-frequency white response, time-domain invariance to rotations, and robustness to frequency errors. Numerical results are provided to assess the behavior of the derived solution.

References

[1] L. Lu, G. Y. Li, A. Maaref, and R. Yao, "Opportunistic transmission exploiting frequency - and spatial-domain degrees of freedom," *IEEE Wireless Commun.*, vol. 21, no. 2, pp. 91–97, Apr 2014.

[2] M. Song, C. Xin, Y. Zhao, and X. Cheng, "Dynamic spectrum access: from cognitive radio to network radio," *IEEE Wireless Commun.*, vol. 19, no. 1, pp. 23–29, Feb 2012.

[3] A. Goldsmith, S. A. Jafar, I. Maric, and S. Srinivasa, "Breaking spectrum gridlock with cognitive radios: An information theoretic perspective," *Proc. IEEE*, vol. 97, no. 5, pp. 894–914, May 2009.

[4] L. Lu, G. Y. Li, and A. Maaref, "Spatial-frequency signal alignment for opportunistic transmission," *IEEE Trans. Signal Process.*, vol. 62, no. 6, pp. 1561–1575, Mar 2014.

[5] H. Yi, H. Hu, Y. Rui, K. Guo, and J. Zhang, "Null space-based precoding scheme for secondary transmission in a cognitive radio MIMO system using second-order statistics," in *IEEE Int. Conf. Commun.*, Jun 2009.

[6] J. Borràs, J. Font-Segura, J. Riba, and G. Vázquez, "Dimension spreading for coherent opportunistic communications," in *2017 51st Asilomar Conf. Signals, Syst. Comput.*, Oct-Nov 2017, pp. 1940–1944.

[7] S. Sodagari, "On effects of imperfect channel state information on null space based cognitive MIMO communication," in *2015 Int. Conf. Comput., Netw., Commun. (ICNC)*, Feb 2015, pp. 438–444.

[8] M. H. Al-Ali and K. C. Ho, "Transmit precoding in underlay MIMO cognitive radio with unavailable or imperfect knowledge of primary interference channel," *IEEE Trans. Wireless Commun.*, vol. 15, no. 8, pp. 5143–5155, Aug 2016.

[9] M. H. Al-Ali and D. K. C. Ho, "Precoding for MIMO channels in cognitive radio networks with CSI uncertainties and for MIMO compound capacity," *IEEE Trans. Signal Process.*, vol. 65, no. 15, pp. 3976–3989, Aug 2017.

[10] R. Zhang and Y. C. Liang, "Exploiting multi-antennas for opportunistic spectrum sharing in cognitive radio networks," *IEEE J. Sel. Topics Signal Process.*, vol. 2, no. 1, pp. 88–102, Feb 2008.

[11] L. Zhang, Y. C. Liang, Y. Xin, and H. V. Poor, "Robust cognitive beamforming with partial channel state information," *IEEE Trans. Wireless Commun.*, vol. 8, no. 8, pp. 4143–4153, Aug 2009.

[12] Y. Zhang, E. DallAnese, and G. B. Giannakis, "Distributed optimal beamformers for cognitive radios robust to channel uncertainties," *IEEE Trans. Signal Process.*, vol. 60, no. 12, pp. 6495–6508, Dec 2012.

[13] S. Trifunovic, S. T. Kouyoumdjieva, B. Distl, L. Pajevic, G. Karlsson, and B. Plattner, "A decade of research in opportunistic networks: Challenges, relevance, and future directions," *IEEE Commun. Mag.*, vol. 55, no. 1, pp. 168–173, Jan 2017.

[14] S. Akin and M. C. Gursoy, "Performance analysis of cognitive radio systems with imperfect channel sensing and estimation," *IEEE Trans. Commun.*, vol. 63, no. 5, pp. 1554–1566, May 2015.

[15] E. M. Dowling and R. D. DeGroat, "The equivalence of the total least square and minimum norm methods," *IEEE Trans. Signal Process.*, vol. 39, no. 8, pp. 1891–1892, Aug 1991.

[16] G. Bienvenu, "Eigensystem properties of the sampled space correlation matrix," in *ICASSP '83. IEEE Int. Conf. Acoust., Speech, Signal Process.*, vol. 8, Apr 1983, pp. 332–335.

[17] M. Wax, T.-J. Shan, and T. Kailath, "Spatio-temporal spectral analysis by eigenstructure methods," *IEEE Trans. Acoust., Speech, Signal Process.*, vol. 32, no. 4, pp. 817–827, Aug 1984.

[18] K. Buckley and L. Griffiths, "Eigenstructure based broadband source location estimation," in *ICASSP '86. IEEE Int. Conf. Acoust., Speech, Signal Process.*, vol. 11, Apr 1986, pp. 1869–1872.

[19] R. Kumaresan and D. W. Tufts, "Estimating the parameters of exponentially damped sinusoids and pole-zero modeling and noise," *IEEE Trans. Acoust., Speech, Signal Process.*, vol. ASSP-30, no. 6, pp. 833–840, Dec 1982.

[20] D. Tufts and R. Kumaresan, "Singular value decomposition and improved frequency estimation using linear prediction," *IEEE Trans. Acoust., Speech, Signal Process.*, vol. 30, no. 4, pp. 671–675, Aug 1982.

[21] R. Kumaresan, "On the zeros of the linear prediction-error filter for deterministic signals," *IEEE Trans. Acoust., Speech, Signal Process.*, vol. 31, no. 1, pp. 217–220, Feb 1983.

[22] S. Jacobsson, G. Durisi, M. Coldrey, T. Goldstein, and C. Studer, "Quantized precoding for massive MU-MIMO," *IEEE Trans. Commun.*, vol. 65, no. 11, pp. 4670–4684, Nov 2017.